Available online at www.sciencedirect.com

ScienceDirect

journal homepage: www.jfda-online.com

Review Article

Electron spin resonance spectroscopy for the study of nanomaterial-mediated generation of reactive oxygen species☆

Weiwei He [a,b], Yitong Liu [b], Wayne G. Wamer [b], Jun-Jie Yin [b,*]

[a] Key Laboratory of Micro–Nano Materials for Energy Storage and Conversion of Henan Province, Institute of Surface Micro and Nano Materials, Xuchang University, Xuchang, Henan, China

[b] Center for Food Safety and Applied Nutrition, US Food and Drug Administration, College Park, MD 20740, USA

ARTICLE INFO

Article history:
Received 30 September 2013
Received in revised form
20 December 2013
Accepted 21 December 2013
Available online 1 February 2014

Keywords:
Electron spin resonance
Lipid peroxidation
Nanomaterials
Reactive oxygen species

ABSTRACT

Many of the biological applications and effects of nanomaterials are attributed to their ability to facilitate the generation of reactive oxygen species (ROS). Electron spin resonance (ESR) spectroscopy is a direct and reliable method to identify and quantify free radicals in both chemical and biological environments. In this review, we discuss the use of ESR spectroscopy to study ROS generation mediated by nanomaterials, which have various applications in biological, chemical, and materials science. In addition to introducing the theory of ESR, we present some modifications of the method such as spin trapping and spin labeling, which ultimately aid in the detection of short-lived free radicals. The capability of metal nanoparticles in mediating ROS generation and the related mechanisms are also presented.

1. Introduction

Rapid development of the nanoscience and technology has produced numerous nanomaterials that offer revolutionary benefits in electronics, energy, medical, and health applications, but unfortunately also lead to environmental, health, and safety concerns [1]. For example, Au nanoparticles (NPs) have been explored as nanopharmaceuticals for the treatment of cancer [2], and Ag NPs have been established as superior antibacterial materials [3]. However, the wide use of nanomaterials has raised concerns regarding their potentially hazardous effects on biological systems, and the associated short- and long-term risks are not well understood. A variety of nanomaterials can generate reactive oxygen species (ROS) under certain experimental conditions [4–9]. Among various toxic responses, nanomaterial-induced oxidative stress mediated by ROS has been studied most extensively [10–12].

ROS, e.g., superoxide, hydroxyl radical, singlet oxygen, and hydrogen peroxide, are powerful oxidants that can damage cellular targets nonselectively. Free radicals, including ROS, are short lived and represent a broad range of chemically distinct entities; consequently, these species are difficult to

☆ This article is not an official US FDA guidance or policy statement. No official support or endorsement by the US FDA is intended or should be inferred.

* *Corresponding author*. Center for Food Safety and Applied Nutrition, US Food and Drug Administration, College Park, MD 20740, USA. E-mail address: junjie.yin@fda.hhs.gov (J.-J. Yin).

http://dx.doi.org/10.1016/j.jfda.2014.01.004

detect in dynamic environments such as biological systems. The use of fluorescent probes (e.g., dichlorodihydrofluorescein, hydroethidine, and dihydrorhodamine) and chemiluminescent assays is a simple and easy way of detecting free radicals and ROS in cellular systems, but there are inherent limitations and many sources of artifacts [13,14]. Electron spin resonance (ESR) spectroscopy has become a powerful and direct method to detect free radicals generated chemically or formed in biological systems. We have a long-standing interest in employing ESR techniques to identify and quantify free radicals in biological systems, and study the mechanisms of interactions between biologically relevant systems and nanomaterials, metal ions, and organic molecules [4,5,7,9,15–43]. We have also published several book chapters on this subject [44–46]. In this special issue, we demonstrate that ESR spectroscopy is a powerful tool for exploring the capability of NPs to generate ROS. The ESR spin-trapping techniques used to detect ROS (including hydroxyl radicals, superoxide radical anion, and singlet oxygen) and the ESR oximetry methodology employed for monitoring oxygen and the formation of lipid peroxidation are also discussed briefly.

2. ESR spectroscopy

2.1. *Principle of ESR spectroscopy*

ESR, also called electron paramagnetic resonance, is a powerful technique for studying chemical species or materials that have one or more unpaired electrons. The basic physical concepts of ESR are analogous to those of nuclear magnetic resonance, except that in ESR electron spins are excited instead of atomic nuclei. ESR has been studied for several decades since it was first observed by Y. Zavoisky in 1944 [47]. A number of review articles and books are available that provide a useful introduction to the basic concepts of ESR and its applications [47–49]. An electron has a spin quantum number $s = 1/2$ with magnetic components $m_s = +1/2$ and $-1/2$. In an external magnetic field, free electrons align with their spin parallel (low energy) or perpendicular (high energy) to the magnetic field (Fig. 1). A transition between low- and high-energy states can occur when sufficient energy is absorbed. This energy lies within the microwave frequencies of the electromagnetic spectrum. The energy ($h\upsilon$) required for this transition is given by the following equation:

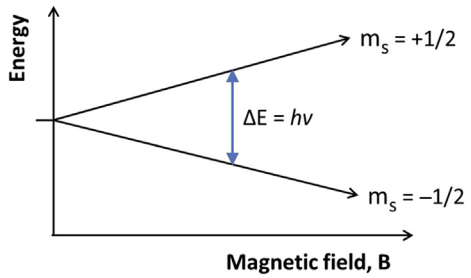

Fig. 1 – Energy diagram showing the origin of an electron spin resonance signal.

$$h\upsilon = g_e \mu_B B_0$$

where μ_B is the Bohr magneton, B_0 is the magnetic field strength, and g_e is the Landé g-factor (2.0023 for free electron). An ESR spectrum is usually obtained by varying the magnetic field strength at a fixed microwave frequency. Magnetic field strengths at which the microwave frequency is absorbed are recorded in the ESR spectrum. A typical continuous wave X-band (9.5 GHz) ESR instrument, as shown in Fig. 2, includes the following major components: (1) a magnet that generates and modulates a magnetic field; (2) a microwave supply system that includes an electromagnetic radiation source and a detector to control the microwave power; (3) a sample cavity to which microwave energies are directed and in which samples are placed; and (4) a data processing and display system. Under certain conditions, each free radical exhibits a specific ESR spectrum, and the intensity of an ESR signal is proportional to the concentration of free radicals; therefore, qualitative identification of free radical species along with their quantitative measurements can be performed.

Spin trapping and spin labeling are the two principal ESR techniques used for the detection and identification of free radicals [9,44,50]. ROS are usually very reactive and present in low concentrations, which is a major limitation to the detection of ROS. However, the instability of free radicals is largely solved by the use of either spin trapping or spin labeling. The ESR spin-trapping technique uses chemical species called spin traps, which react with short-lived free radicals to form relatively stable adducts having a half-life long enough for ESR measurement [50]. The ESR spin-labeling technique uses a stable paramagnetic spin label agent to interact with the target chemical, e.g., the oxygen molecule or electrons, and is a powerful tool for probing structural and/or dynamic changes in complex chemical or biological systems [51,52]. Here, our discussion focuses on oxygen-centered free radicals, particularly ROS. In this review, carbon- and sulfur-centered free radicals have not been included.

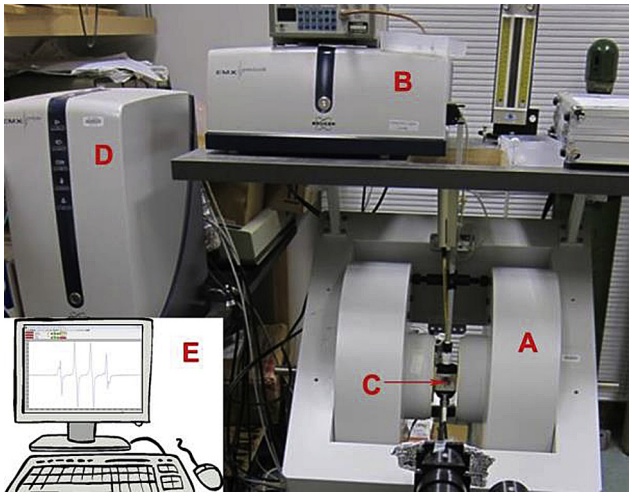

Fig. 2 – Photograph of a typical Bruker EMX continuous-wave electron spin resonance instrument. The components A, B, C, D, and E represent magnet, microwave supply and control system, sample cavity, data processing, and display system, respectively.

2.2. *ESR spin-trapping technique*

There are three kinds of spin traps, compounds with nitrone, nitroso, and piperidine/pyrrolidine groups [50], as displayed in Fig. 3. Most of these spin traps are soluble in water and polar organic solvents, can capture a variety of free radicals, and can reveal specific hyperfine splitting information, which aids in the identification of radicals. Nitrone spin traps include cyclic and open-chain nitrones. Spin traps including 5,5,-dimethylpyrroline N-oxide (DMPO), 5-tertbutoxycarbonyl-5-methyl-1-pyrroline N-oxide (BMPO), 5-diethoxyphosphoryl-5-methyl-1-pyrroline-N-oxide (DEPMPO), and other derivatives have similar cyclic nitrone structures and are highly useful for trapping oxygen-centered free radicals, including superoxide and hydroxyl radicals. Phenyl-tert-butylnitrone and α-(4-pyridyl N-oxide)-N-tert-butylnitrone (POBN) are common open-chain nitrone spin traps, which are typically used to trap carbon-centered free radicals. Nitrone spin traps can capture the radical at a carbon adjacent to the nitrogen, which results in the loss of chemical information. However, the most popular spin traps have a β-hydrogen that can provide considerable qualitative information about the trapped radicals. DMPO, BMPO, and DEPMPO can be used to trap hydroxyl radicals and superoxide, forming adducts with •OH or •OOH. However, in the detection of superoxide using DMPO as a spin trap, the resulting DMPO/•OOH adducts are unstable and decay to DMPO/•OH adducts, leading to a misinterpretation of the generation of hydroxyl and superoxide radicals [53]. The spin adducts BMPO/•OOH and DEPMPO/•OOH are highly stable, especially BMPO/•OOH that does not decompose into the corresponding hydroxyl adduct.

Nitroso spin traps such as 2-methyl-2-nitrosopropane and nitrosobenzene, and their derivatives, can provide more

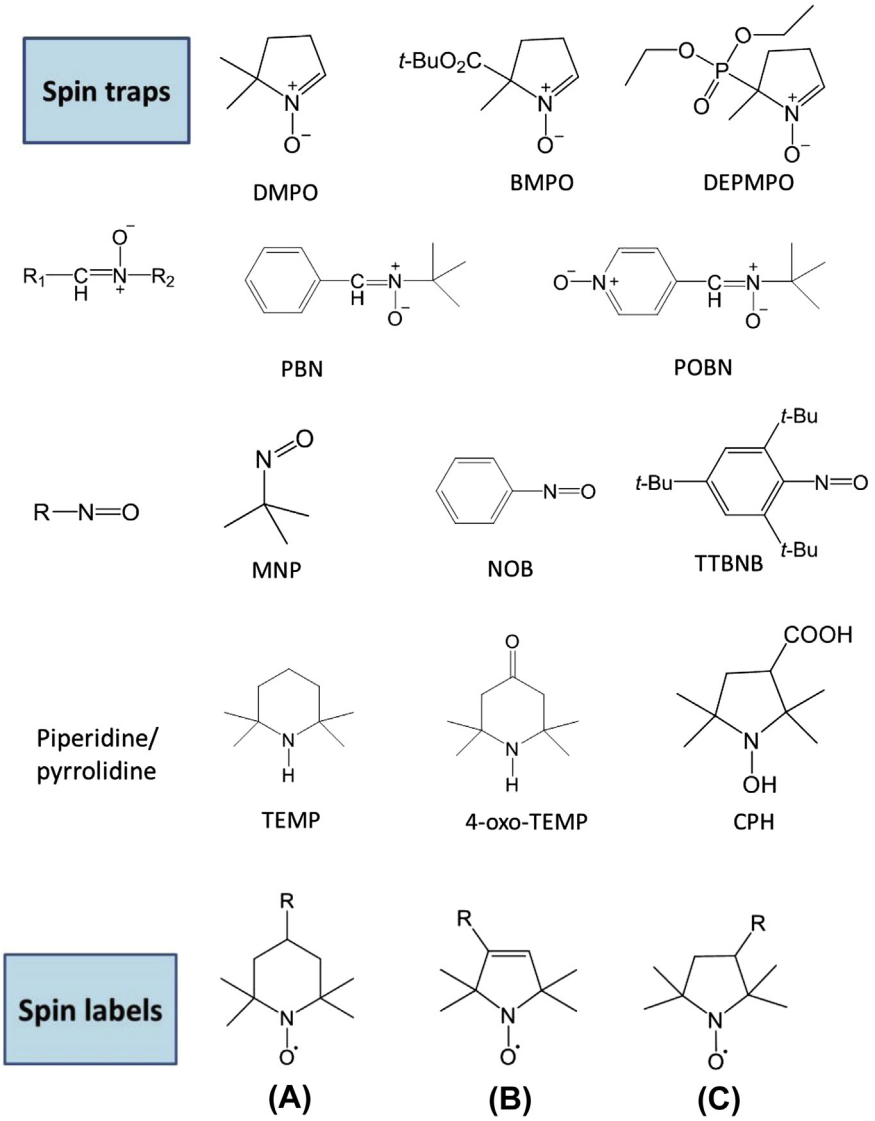

Fig. 3 – Chemical structures of common spin traps and spin labels including (A) a piperidine nitroxide derivative, (B) an unsaturated pyrrolidine nitroxide derivative, and (C) a saturated pyrrolidine nitroxide derivative. BMPO = 5-tertbutoxycarbonyl-5-methyl-1-pyrroline N-oxide; CPH = 1-hydroxy-3-carboxy-pyrrolidine; DEPMPO = 5-diethoxyphosphoryl-5-methyl-1-pyrroline-N-oxide; DMPO = 5,5-dimethylpyrroline N-oxide; MNP = 2-methyl-2-nitrosopropane; NOB = nitrosobenzene; PBN = phenyl-tert-butylnitrone; POBN = α-(4-pyridyl N-oxide)-N-tert-butylnitrone; TEMP = 2,2,6,6-tetramethylpiperidine; TTBNB = 2,4,6-tri-tert-butylnitrosobenzene.

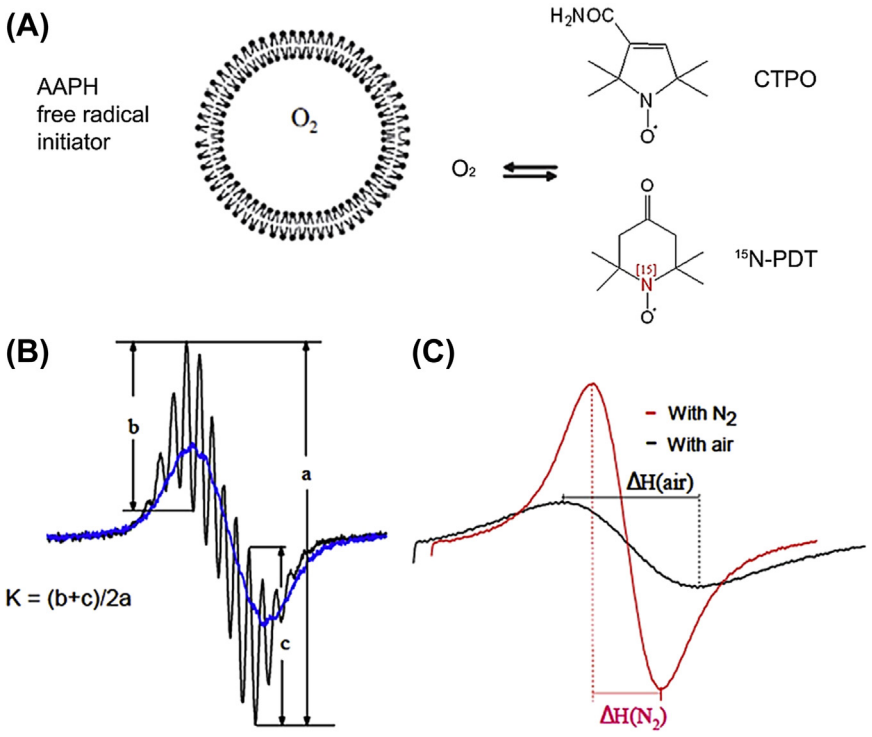

Fig. 4 – Measurement of oxygen by ESR oximetry. (A) Oxygen consumption is measured in a closed chamber using liposome suspensions and the spin label ^{15}N-PDT mixed with a free radical initiator of lipid peroxidation such as AAPH. (B) The black line indicates ESR spectra of CTPO in a nitrogen-saturated aqueous solution and the blue line indicates that in an air-saturated aqueous solution; the *K* parameter is used to determine oxygen concentration and is calculated by the equation $K = (b + c)/2a$. (C) The ESR spectra of ^{15}N-PDT in a nitrogen atmosphere is shown by the red line and that in an air-saturated aqueous solution is shown by the black line. The presence of oxygen results in a broader and less intense ESR signal for the spin probe [57]. CTPO = 3-carbamoyl-2,2,5,5-tetra-methyl-3-pyrroline-1-yloxyl; ESR = electron spin resonance; ^{15}N-PDT = 4-oxo-2,2,6,6-tetramethyl piperidine-d_{16}-1-^{15}N-oxyl; AAPH = 2,2′-azobis(2-amidino-propane)dihydrochloride.

information than nitrones because the radical to be trapped adds directly to the nitroso nitrogen. However, these spin traps are not suitable for studying oxygen-centered radicals because their resulting spin adducts are photochemically and thermally unstable [53].

Representative piperidine-based spin traps, 2,2,6,6-tetramethylpiperidine (TEMP) and 4-oxo-2,2,6,6-tetramethyl piperidine (4-oxo-TEMP), can be specific traps for reacting with singlet oxygen to yield a nitroxide radical TEMPONE with a stable ESR signal, as shown in reaction (1) [9]. Consequently, TEMP has widely been used in ROS characterization for the detection of singlet oxygen. The spin trap 1-hydroxy-3-carboxy-pyrrolidine (CPH) was found to be more suitable than 1-hydroxy-2,2,6,6-tetramethyl-4-oxo-piperidine (TEMPONE-H) for trapping superoxide radicals and peroxynitrite in biological systems [54]. CPH reacts with superoxide radicals or peroxynitrite forming the stable nitroxide radical 3-carboxy-2,2,5,5-tetramethylpyrro lidine 1-oxyl, which can be detected by ESR spectroscopy.

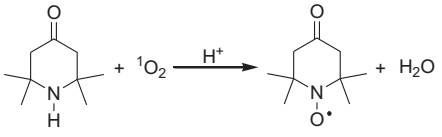

(1)

TEMP TEMPONE

2.3. *ESR spin-labeling technique*

Spin labels are stable nitroxide free radicals, which possess an unpaired electron that has the ability to bind to another molecule. The magnetic resonance signal of this unpaired electron can be detected by ESR, which would provide information about the motion, distance, and orientation of unpaired electrons in the sample with respect to each other and to the external magnetic field. ESR spin labeling is particularly useful in the field of biology for probing local dynamics of proteins or biological membranes [55]. Most spin labels are derived from five- or six-membered hybrid rings (Fig. 3), with various functional groups indicated by R [45,56]. For example, commonly used spin labels 2,2,6,6-tetramethyl-1-piperidinyloxy, 2,2,6,6-tetramethylpiperidine 1-oxyl (TEMPO, R = H), 2,2,6,6,-tetramethyl-4-piperidone-1-oxyl (TEMPON, R = oxo), 4-hydroxy-2,2,6,6-tetramethylpiperidine 1-oxyl (TEMPOL, R = OH), and 4-amino-2,2,6,6-tetramethyl piperidine-1-oxyl (4-amino-TEMPO, R = NH_2) are derived from the piperidine structure (Fig. 3A). The spin labels 3-carbamoyl-2,2,5,5-tetra-methyl-3-pyrroline-1-yloxyl (CTPO) and (1-oxyl-2,2,5,5-tetramethyl-Δ^3-pyrroline-3-methyl) methanethiosulfonate have the same pyrroline structure with different R groups. 3-Carboxy-2,2,5,5-tetramethylpyrrolidine 1-oxyl is one representative free radical from saturated pyrrolidine structure (Fig. 3C). These nitroxide free radicals have

Table 1 – Generation of ROS mediated by metal NPs, based on the data from previous reports.

NPs	ROS production	Experimental conditions and detection methods	Refs
Ag	•OH	0.5 mM H_2O_2, pH < 4.5, 10–100 nm, different coatings, ESR	[4]
	ROS, •OH	9–21 nm, with light, fluorescence	[60]
	ROS	In cell, 15–55 nm, fluorescence	[61]
	ROS	In human liver cell, 5–10 nm, fluorescence	[62]
	Free radicals	10 nm, ESR	[63]
	ROS	In cell, 6–20 nm, fluorescence	[64]
	O_2^{-}•	Protein/membrane, SOD	[65]
	O_2^{-}•	1.0 M KOH, H_2O_2, Al supported, ESR	[66]
	ROS	In cell, 25–70 nm, fluorescence	[67]
	ROS	Intracellular, PVP coated, 70 nm, fluorescence	[68]
	•OH, O_2^{-}•	Under UV, fluorescence	[6]
	O_2^1	Ag NPs, photoirradiation, fluorescence	[8]
Au	•OH	0.5mM H_2O_2, pH < 3.6, 10–100 nm, different coatings, ESR	[5]
	O_2^1	Under UV, fluorescence	[6]
	O_2^1	Au NPs, photoirradiation (NIR), fluorescence	[8]
	ROS	Under laser pulse irradiation, in cell, fluorescent marker	[2]
	ROS	Protoporphyrin IX coated, under light, fluorescence	[69]
	•OH, O_2^{-}•	2–250 nm, X-ray and UV irradiation, fluorescence	[70]
Pt	•OH	Pt surface, H_2O_2, under high-voltage power supply	[71]
$CoPt_3$	•OH, O_2^{-}•	0.11M H_2O_2, ESR	[72]
FePt	ROS	In cell, PBS, fluorescence	[73]
Cu	ROS	Mercaptocarboxylic acid coated, 15 nm, fluorescence	[74]
	•OH	1mM H_2O_2, 1mM PBS, ESR	[75]
	O_2^1	4–5 nm, PBS, citrate coated, by NaN_3, fluorescence	[76]
Fe	•OH	O_2, pH < 5, fluorescence	[77,78]
	O_2^{-}•	O_2, PBS, in cell, fluorescence	[79]
	ROS	*Escherichia coli*, fluorescence	[80]
	•OH	28mM H_2O_2, ESR	[81]
FeCo	•OH	28mM H_2O_2, ESR	[81]
Co	•OH	28mM H_2O_2, ESR	[81]
	ROS	Dose dependent, in cell, fluorescence	[82]
Ni	O_2^1	Under UV, fluorescence	[6]
	ROS	~30 nm, in human liver cell, fluorescence	[83]
	ROS	65 nm, human lung epithelial A549 cells, fluorescence	[84]

ESR = electron spin resonance; NP = nanoparticle; PBS = phosphate-buffered saline; PVP = polyvinylpyrrolidone; ROS = reactive oxygen species; SOD = superoxide dismutase; NIR = near infrared.

the advantage of high sensitivity and unambiguous spectral information. A concentration of 1 μM TEMPO in a 50 μL volume can be detected easily by conventional ESR.

Spin label oximetry is a highly useful method to detect dissolved oxygen in biological environments [56]. Spin label oximetry is based on the bimolecular collision between oxygen (O_2) and spin labels. As O_2 is paramagnetic, a physical collision between the spin label and O_2 produces a Heisenberg spin exchange, which results in a shorter relaxation time leading to a broader line width and lower peak intensity in the ESR spectrum of the spin label. Because the extent of spin exchange is dependent on the concentration of molecular O_2, a change in O_2 concentration results in a corresponding change in the line width of the spin label. Therefore, a real-time study of O_2 generation or consumption is feasible in biological systems. The most commonly used spin labels in oximetry are CTPO and 4-oxo-2,2,6,6-tetramethyl piperidine-d_{16}-1-^{15}N-oxyl (^{15}N-PDT; Fig. 4). Their ESR spectral shapes are dependent on the amount of O_2 molecule interacting with spin labels. Practically, CTPO, because of its superhyperfine structure in the ESR spectrum, is more sensitive to O_2 than ^{15}N-PDT. The choice of spin labels is dependent on the O_2 concentration. The spin label ^{15}N-PDT is suitable for use at a high O_2 concentration (>150 mM), whereas CTPO is preferred at a low O_2 concentration. A limit of detection for molecular oxygen of 0.1 μM can be achieved using the CTPO spin label oximetric method [57]. By repeatedly measuring the line widths of the spin probe, one can assess the rate of lipid peroxidation in the biological sample (Fig. 4).

3. ROS generation mediated by metal NPs

Owing to the quantum size effect, nanomaterials possess unique physiological and chemical properties that are different from those in either macroscopic (bulk) or atomic form. Concerns have been raised that these unique properties may lead to nanomaterial-induced toxicity. A variety of nanomaterials, including metal NPs, carbon nanostructures, and semiconductor NPs, have been shown to be toxic to living systems. One important mechanism of nanomaterial-induced toxicity is the generation of ROS. In this special issue, a review article by Fu et al [58], titled "Mechanism of Nano-toxicity—Generation of Reactive Oxygen Species," discusses the mechanisms and decisive determinants of the generation of ROS by nanomaterials. As an illustration for this review, we

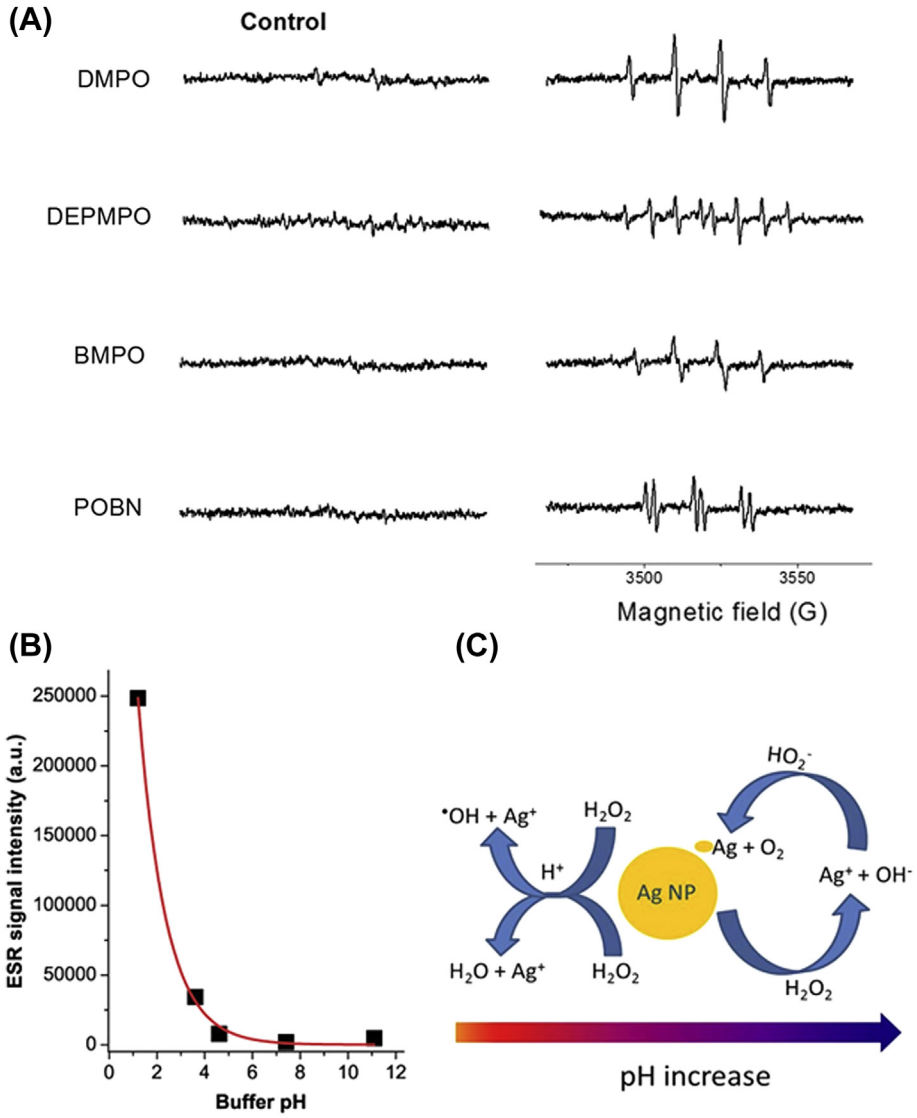

Fig. 5 – (A) Demonstration of hydroxyl radicals generated by Ag NPs in the presence of hydrogen peroxide at pH 3.6 (10mM acetate buffer) using different spin traps. (B) ESR signal intensity versus buffer pH. (C) Schematic presentation of Ag NPs triggering the generation of hydroxyl radicals and oxygen controlled by pH [4]. BMPO = 5-tertbutoxycarbonyl-5-methyl-1-pyrroline N-oxide; DEPMPO = 5-diethoxyphosphoryl-5-methyl-1-pyrroline-N-oxide; DMPO = 5,5-dimethylpyrroline N-oxide; ESR = electron spin resonance; NP = nanoparticle; POBN = α-(4-pyridyl N-oxide)-N-tert-butylnitrone.

focus our presentation on the generation of ROS mediated by metal NPs.

A variety of metal NPs have been reported to exhibit intrinsic activity in generating or scavenging ROS. Some representative results are summarized in Table 1, including NPs of metals Ag, Au, Pt, Cu, Fe, Co, Ni Fe, and Co [4–6,60–84]. Ag, Au, Cu, Fe, Ni, and Co NPs have been reported for their ability to induce the generation of ROS under certain experimental conditions. Au NPs generate ROS, including •OH, O_2^1, and O_2^{-}•, in various environments [2,5,6,8,69,70], whereas Ag NPs enable the production of •OH and O_2^{-}• [4,6,8]. Cu NPs have been reported to generate •OH in the presence of hydrogen peroxide [75] and proposed to form O_2^1 when present with DNA in phosphate-buffered saline [76]. Most of these studies used fluorescent probes, instead of ESR, to measure ROS and reported only the total ROS production-related oxidative stress [61,62,64,67–69,73,74,82–84]. These studies indicate that physiochemical factors, including the size, shape, composition, and surface coating, of metal NPs affect ROS levels significantly. ROS production occurs mainly through two mechanisms: (1) Fenton-like reaction and (2) surface plasmon resonance enhancement; both of these are discussed in detail in the following subsections.

3.1. *ROS generation via Fenton reaction*

A Fenton or Fenton-like reaction is a process that leads to the generation of hydroxyl radicals, as illustrated in reaction (2), which is best exemplified by reactions between H_2O_2 and

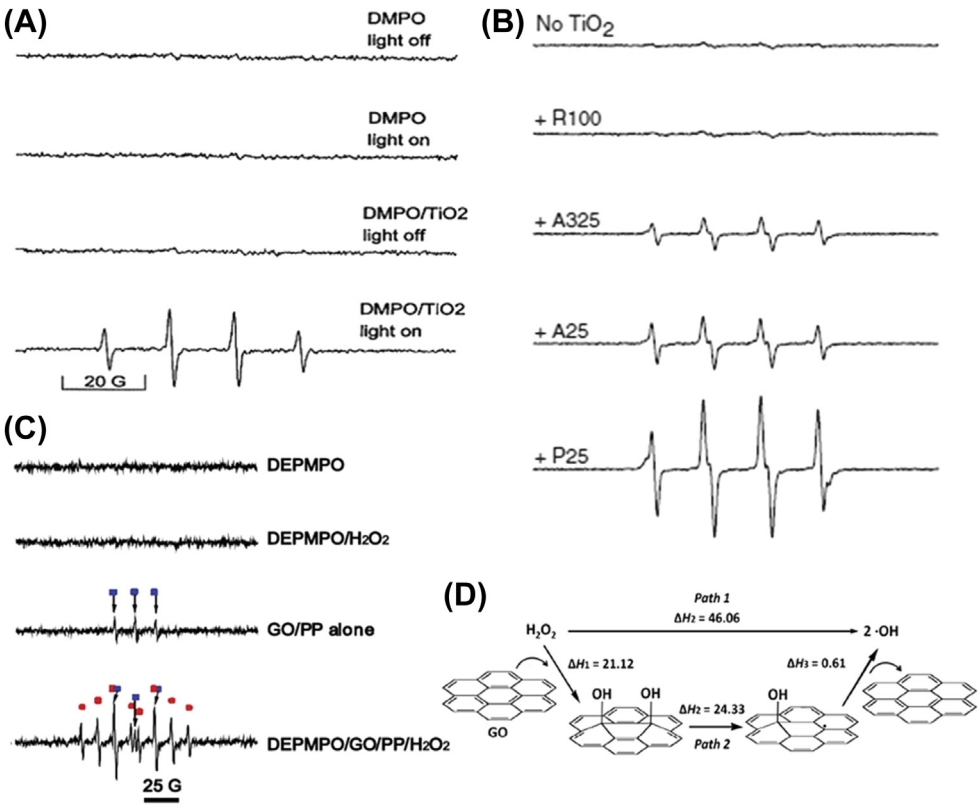

Fig. 6 – Generation of hydroxyl radicals by irradiation of TiO_2 samples under UV light. ESR spectra (A) with DMPO recorded after 3 minutes of irradiation with UV radiation of 320 nm [89], and (B) with BMPO after 2 minutes of irradiation with UV 340 nm [9]. (C) Catalytic activity of GO/PP in the formation of ·OH by decomposition of H_2O_2, using DEMPO as a spin trap. (D) A possible decomposition mechanism of hydrogen peroxide catalyzed by coronene [94]. BMPO = 5-tertbutoxycarbonyl-5-methyl-1-pyrroline N-oxide; DEPMPO = 5-diethoxyphosphoryl-5-methyl-1-pyrroline-N-oxide; DMPO = 5,5-dimethylpyrroline N-oxide; ESR = electron spin resonance; GO/PP = graphene oxide modified with PEGylated poly-L-lysine.

Fenton-like reagents involving transition metal ions such as Fe^{2+} and Cu^{+} [59]:

$$H_2O_2 + M^{n+} \rightarrow M^{n+1} + {}^{\bullet}OH + OH^{-} \quad (2)$$

Zero-valent metal NPs with relatively low redox potentials, such as Ag, Cu, and Fe NPs, can be viewed as Fenton-like NPs. They all have redox potentials less than that of H_2O_2/H_2O (1.77 V). For example, elemental silver ($\varphi_{Ag+/Ag} = +0.7996$ V), copper ($\varphi_{Cu+/Cu} = 0.52$ V, and $\varphi_{Cu2+/Cu} = 0.34$ V), and iron ($\varphi_{Fe2+/Fe} = -0.44$ V) are thermodynamically favorable to trigger the Fenton reaction in the presence of H_2O_2, as displayed in reaction (3) [4]:

$$M(NP) + H_2O_2 + nH^{+} = M^{n+} + {}^{\bullet}OH + H_2O \quad (3)$$

Therefore, a Fenton reaction is always accompanied by oxidation and dissolution of metal NPs. Dissolved metal ions such as Fe^{2+} and Cu^{+} can further promote the Fenton reaction shown in reaction (2).

He and coworkers [4] have reported the hydroxyl radicals generated from the interaction between H_2O_2 and Ag NPs. The formation mechanism of hydroxyl radical was suggested to take place through a Fenton reaction between Ag NPs and H_2O_2. Therefore, they named Ag NPs as Fenton-like NPs. Cu NPs may go through a similar process to generate hydroxyl radicals, as indicated in another study, although the authors of the study did not make such a proposal [75]. Zero-valent Fe NPs not only trigger the Fenton reaction in the presence of H_2O_2 to form hydroxyl radicals, but also activate dissolved oxygen to produce superoxide and H_2O_2, which can generate hydroxyl radicals [77–79,81]. Reactive oxygen production at neutral and alkaline pH is typically lower than that at acidic pH, due to the precipitation of metal ions and the mechanism involved in the Fenton reaction. Spherical Co and FeCo alloyed NPs were investigated by ESR spectroscopy, using DMPO as a spin trap, to generate hydroxyl radicals in the presence of 28 mM H_2O_2 through a Fenton-like reaction [81]. Bimetallic NPs such as CoPt and FePt were also found to produce ROS (hydroxyl radicals and superoxide) in the presence of H_2O_2 due to leaching of active metal ions (Fe and Co) from the particle surface, triggering a Fenton reaction [72,73].

3.2. *Surface plasmon resonance enhancement*

Because metal NPs contain free electrons, they can interact with an incident electromagnetic wave, resulting in the collective oscillation of electrons. When the frequency of the

incident light photons equals the oscillating frequency of electrons, a resonance phenomenon, called localized surface plasmon resonance, occurs [85]. A local enhanced electromagnetic field formed on the surface of metal NPs makes the NPs useful not only in optical sensing and imaging [86], but also in enhancing the generation of ROS [2,6,8,69,70]. Zhang and coworkers [6] found that, under UV irradiation (365 nm), Ag NPs generated superoxide and hydroxyl radicals, whereas Au NPs and Ni NPs generated only singlet oxygen. They proposed that the ROS generation from Au, Ag, and Ni was primarily due to surface plasmon resonance effects. In another study, Vankayala et al [8] reported that both Ag and Au NPs can generate singlet oxygen upon photoirradiation of the surface plasmon resonance band, even at near-infrared wavelengths. Researchers characterized and quantified, using different fluorescent markers, the significant elevation in ROS generation from antibody-coated Au NPs irradiated by a few resonant femtosecond laser pulses, which resulted in a high concentration of ROS and local damage of cancer cells [2]. Au NPs can also enhance and improve the generation of ROS from photosensitizers located near the Au NP surface. Oo et al [69] have demonstrated that ROS formation by Au NPs is significantly enhanced upon irradiation with a PpIX photosensitizer because of the localized electromagnetic field of surface plasmon resonance of the illuminated Au NPs. They also found that ROS enhancement, leading to damage of breast cancer cells, is proportional to the size of Au NPs. Additionally, photo- and Auger-electron charge transfer may influence the generation of $O_2^{-}\bullet$ near the Au NP surface, whereas X-rays are involved in the generation of •OH [70].

4. Application of ESR for the detection of ROS generated by nanomaterials

4.1. *Application of ESR spin trapping for the detection of hydroxyl radicals mediated by nanomaterials*

Hydroxyl radicals are extremely reactive and can cause oxidative damage to a majority of macromolecules in biological systems [87]. A hydroxyl radical has a very short half-life (about 1 nanosecond) and a high reactivity [88], which makes its detection challenging. However, they readily react with diamagnetic nitrone spin traps, forming stable free radicals (spin adducts) that can be identified from the magnetic parameters of the ESR spectrum. We have used ESR spin trapping to study the generation of hydroxyl radicals by Ag and Au NPs during their interactions with H_2O_2 [4,5]. Four spin traps, DMPO, BMPO, DEPMPO, and POBN, were employed to characterize the generation of hydroxyl radicals in the presence of H_2O_2 and Ag NPs under acidic conditions (pH 3.6; Fig. 5). Compared with control conditions, we observed ESR spectra characteristic of adducts formed between each of the four spin traps and hydroxyl radicals, indicating that hydroxyl radicals are generated when the decomposition of hydrogen peroxide is assisted by Ag NPs under acidic conditions. Most notably, the generation of hydroxyl radical is dependent not only on the size and concentration of Ag NPs, but also on the buffer pH, as shown in Fig. 5. The pH dependence and Ag NP induction of hydroxyl radical generation were suggested to be due to the pH-dependent redox behavior of H_2O_2 and the ability of Ag NPs to facilitate electron transfer in different chemical environments (Fig. 5C). By employing spin-trapping ESR, we also demonstrated that Au NPs can facilitate generation of hydroxyl radicals in the presence of hydrogen peroxide [5], the pH dependence being similar to Ag NPs.

Metal oxide NPs, for example TiO_2 and ZnO, are photocatalytically active and generate ROS when photoexcited. Under some experimental conditions, particularly those found in *in vitro* studies, this photochemical activity can lead to cytotoxicity [9,89–91]. We employed DMPO or BMPO as a spin trap to determine whether hydroxyl radicals can be produced from irradiated TiO_2 and ZnO NPs [89–91]. When TiO_2 is irradiated with UV in the presence of DMPO, an ESR spectrum characteristic of the spin adduct DMPO/•OH is observed (Fig. 6A) [89]. Using BMPO as a spin trap, we further examined the generation of hydroxyl radicals for different crystalline types of TiO_2. The results showed that rutile, anatase, and P25 all can produce hydroxyl radicals when irradiated, while irradiation of P25 results in the strongest signal of BMPO/OH (Fig. 6B) [9]. Similarly, ZnO NPs can generate hydroxyl radicals in a dose-dependent manner when exposed to UVA radiation, which may result in the death of human-derived keratinocytes [91]. In our collaborative work with other groups, we performed ESR spectroscopy and demonstrated that iron oxide NPs (e.g., Fe_2O_3 and Fe_3O_4 NPs) can induce the formation of hydroxyl radicals in an acidic biological microenvironment through Fenton or Fenton-like reactions [7,92].

In collaboration with Zhao et al [93,94], we employed ESR to study the ability of carbon nanostructures, such as carbon nanotubes and graphene oxide, to generate hydroxyl radicals. Using DMPO as a spin trap, hydroxyl radicals were generated using carbon nanotubes by interaction with H_2O_2. This generation of hydroxyl radicals may be caused by the existence of carbonaceous and transition metallic impurities (e.g., Fe) [93]. In the study of graphene oxide (GO), functionalized GO modified with PEGylated poly-L-lysine (GO/PP) was found to catalyze the decomposition of H_2O_2 to form hydroxyl radicals. The hydroxyl radicals were captured by DEMPO and detected by ESR (Fig. 6C). A theoretical calculation suggests a possible decomposition mechanism of hydrogen peroxide catalyzed by coronene (Fig. 6D) [94].

4.2. *Application of ESR spin trapping for the detection of superoxide anion radicals generated by nanomaterials*

Among the spin traps, DMPO and BMPO are used most often for detecting superoxide anions. Harbour and Hair [95] have detected the superoxide generated from photoexcited CdS dispersions using DMPO as a spin trap. The ESR technique along with the spin trap DMPO was also used by Wang et al [96] for studying illuminated $CdIn_2S_4$ microspheres. These investigators observed the characteristic peaks of the DMPO/$O_2^{-}\bullet$ adducts in methanol dispersion under irradiation. Zhao et al [53] have shown that use of the spin trap BMPO has advantages over DMPO as a spin trap for superoxide. This is because the BMPO/•OOH adduct is more stable and does not decompose into the corresponding hydroxyl adduct (i.e.,

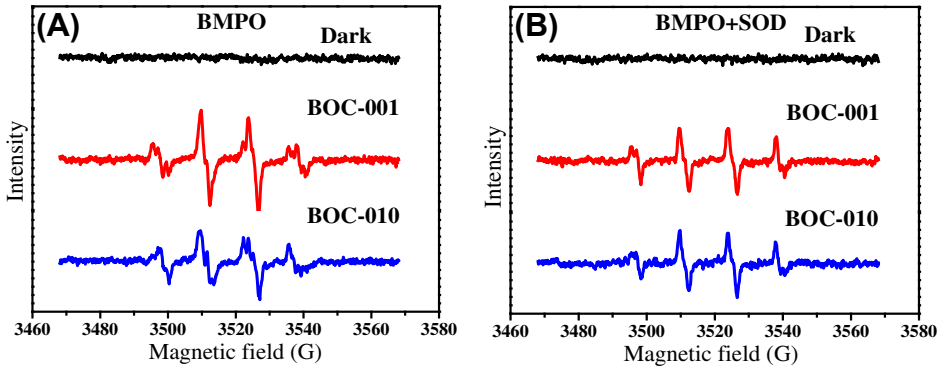

Fig. 7 – ESR spectra of active oxygen radicals generated during the photocatalysis of BOC-001 and BOC-010 under UV irradiation (A) prior to and (B) after the addition of SOD [97]. BMPO = 5-tertbutoxycarbonyl-5-methyl-1-pyrroline N-oxide; BOC-001 = BiOCl with dominantly exposed face 001; BOC-010 = BiOCl with dominantly exposed face 010; ESR = electron spin resonance; SOD = superoxide dismutase.

BMPO/•OH). However, the spin adducts BMPO/•OOH and BMPO/•OH have overlapping ESR spectra, and so also the ESR spectra for DMPO/•OOH and DMPO/•OH. Therefore, it is difficult to distinguish between hydroxyl radicals and superoxide if they are generated simultaneously in one system. An examination of the quenching effect of superoxide dismutase (SOD) on superoxide or that of DMSO on hydroxyl radicals can provide additional confirmation of the existence of these free radicals. Zhao et al [97] have reported that excitation of BiOCl nanostructures with UV results in the appearance of a strong four-line ESR spectrum with splitting parameters of $a^{N} = 13.56$, $a^{\beta}_{H} = 12.30$, and $a^{\gamma}_{H} = 0.66$, which is the characteristic spectrum of BMPO/•OH adduct. Similar results were obtained for BiOCl with dominantly exposed faces 001 (BOC-001) and 010 (BOC-010). The superoxide was also captured to form the BMPO/O_2^{-}• adduct having a four-line spectrum with relative intensities of 1:1:1:1 and hyperfine splitting parameters of $a^{N} = 13.56$ and $a^{\beta}_{H} = 12.10$, which overlaps with the BMPO/•OH spectrum. To verify whether the ESR signal involved superoxide, SOD was added. After the addition of SOD, the ESR signal intensity decreased; however, no similar decrease was observed for BOC-001 and BOC-010 (Fig. 7). These observations indicated that although both •OH and O_2^{-}• were generated from irradiated BOC, •OH dominated, resulting in the unclear characteristic ESR signal for O_2^{-}• [97].

4.3. *Application of ESR spin trapping for the detection of singlet oxygen generated by nanomaterials*

Singlet O_2 is a very important ROS involved in peroxidation of olefins, photobiological cytotoxicity, and, importantly, clinical photodynamic therapy for killing cancer cells. Upon irradiation, a variety of nanomaterials, including metal NPs (Au, Ag, Ni, etc.) [6,8], semiconductor NPs (Si, TiO_2, ZnO, etc.) [9,41,98], and fullerenes [39,40], can efficiently generate singlet oxygen. Singlet oxygen can be formed by photoexcitation of metal NPs due to their surface plasmon resonance properties. For example, Au nanorods generate singlet oxygen via photoexcitation in the near-infrared region, which may potentially lead to their use in photodynamic and photothermal therapies for cancer treatment [8]. Additionally, semiconductor NPs such as TiO_2, ZnO, etc. are well-known photocatalysts. Because of their electronic structure, these materials are capable of generating singlet oxygen on photoexcitation. As discussed in Part 2.2, TEMP and 4-oxo-TEMP are two typical spin traps used for the detection of singlet oxygen in ESR. We have examined the generation of singlet oxygen from irradiated TiO_2 by the ESR trapping technique using TEMP [9]. Irradiation of different nanoscale TiO_2 samples containing 20 mM TEMP resulted in an ESR spectrum consisting of three lines with equal intensities ($a_N = 16.0$ G), which is typical of nitroxide radicals (Fig. 8, inset). The hyperfine splitting constant

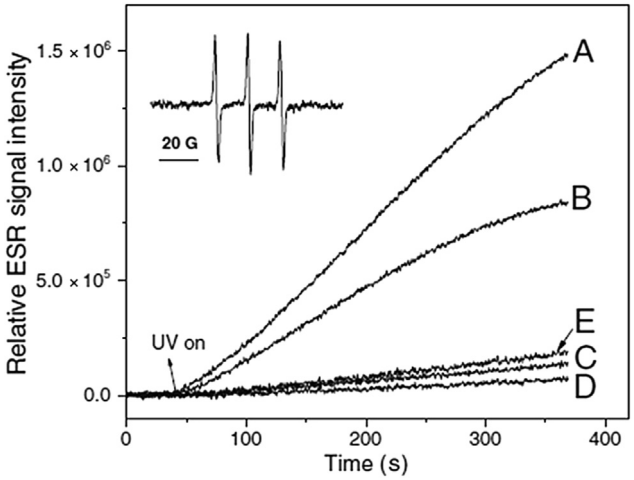

Fig. 8 – Generation of singlet oxygen by photoexcitation of TiO_2 samples under UVA light in time- and crystal type-dependent manners. ESR spectra were recorded at room temperature. Samples containing 20mM TEMP and 0.1 mg/mL P25 (curve A), 0.1 mg/mL A25 (curve B), 0.1 mg/mL A325 (curve C), and 0.1 mg/mL R100 (curve D), and that containing 10 mM NaN_3 and 0.1 mg/mL P25 (curve E) were irradiated with UVA light at 340 nm. Inset: ESR signal of TEMPONE ($a_N = 16.0$ G) [9]. ESR = electron spin resonance; TEMP = 2,2,6,6-tetramethylpiperidine.

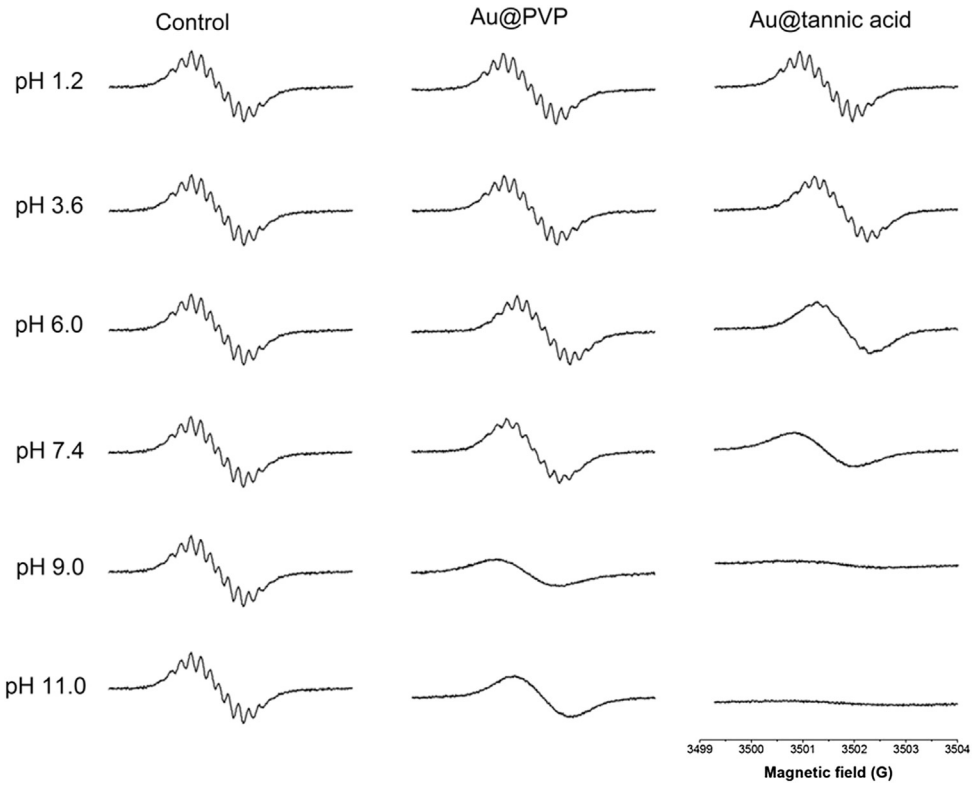

Fig. 9 – Generation of O_2 induced by Au NPs under different experimental conditions. ESR spectra of 0.1mM CTPO in 10 mM buffers having different pH, in the presence of 0.5 mM H_2O_2 and 0.1 mg/mL Au NPs (particle size 10 nm). Sample solutions were aerated with nitrogen for 15 minutes prior to mixing. ESR spectra were collected after 6 minutes of incubation [5]. CTPO = 3-carbamoyl-2,2,5,5-tetra-methyl-3-pyrroline-1-yloxyl; ESR = electron spin resonance; NP = nanoparticle; PVP = polyvinylpyrrolidone.

and *g* factor are characteristic of TEMPONE. The ESR intensity of the TEMPONE signal increased as a function of time during irradiation of different nano-TiO_2 samples. A control solution containing only TEMP did not lead to an increase in the ESR signal. For P25 nano-TiO_2, the addition of a singlet oxygen quencher, NaN_3, caused a significant reduction in the rate of increase of the electron paramagnetic resonance signal (Fig. 8, curve E). The rates of production of singlet oxygen for the different species followed the trend P25 > A25 > A325 > R100 nano-TiO_2 (Fig. 8).

Zhao et al [41] studied the encapsulation of silicon phthalocyanine 4 (Pc4) in silica NPs to enhance photodynamic efficacy toward melanoma cells. Using the spin trap TEMP, they showed that photoexcited Pc4 encapsulated in silica NPs, with a particle size in the range of 25–30 nm, generated singlet oxygen. Intensity of the ESR signals from TEMPONE was enhanced progressively when the irradiation time was extended. These results provide direct evidence that the photoexcitation of Pc4 encapsulated in silica NPs with visible light (>550 nm) generates singlet oxygen and that the quantity of singlet oxygen formed is dependent on the dose of administered light. In addition to Pc4 and silica NPs, fullerenes were also studied. The water-soluble fullerene derivative γ-cyclodextrin bicapped C_{60} [$(\gamma\text{-CyD})_2/C_{60}$, CDF0] was found to be a highly efficient photosensitizer for the generation of singlet oxygen. In a study assessing its potential phototoxicity in human lens epithelial cells (HLE B-3) *in vitro*, using the same ESR/TEMP trapping technique, Zhao et al [40] found that $(\gamma\text{-CyD})_2/C_{60}$ (CDF0) can produce singlet oxygen efficiently. A solution of $(\gamma\text{-CyD})_2/C_{60}$ (CDF0) showed the highest rate of singlet oxygen production; the rate decreased with increasing aggregation, with no production by the fully aggregated sample after 150 minutes of heating (CDF150). They concluded that singlet oxygen is an important intermediate in the phototoxicity of monomeric $(\gamma\text{-CyD})_2$/fullerene.

4.4. *Application of ESR spin label oximetry for studying lipid peroxidation by nanomaterials*

In the detection of O_2, ESR oximetry has a number of advantages. For example, ESR oximetry does not lead to consumption of O_2 during measurement and it is nondestructive. In addition, ESR oximetry has less interference with small molecules and requires less sample volume while maintaining high sensitivity [57]. Chemically, lipid peroxidation can be caused by O_2, light, ROS, and other free radicals. Importantly, lipid peroxidation is associated with the consumption of O_2. Therefore, ESR spin label oximetry is very suitable for sensitive detection of lipid oxidation by measuring O_2 consumption. In addition, ESR oximetry can also provide dynamic

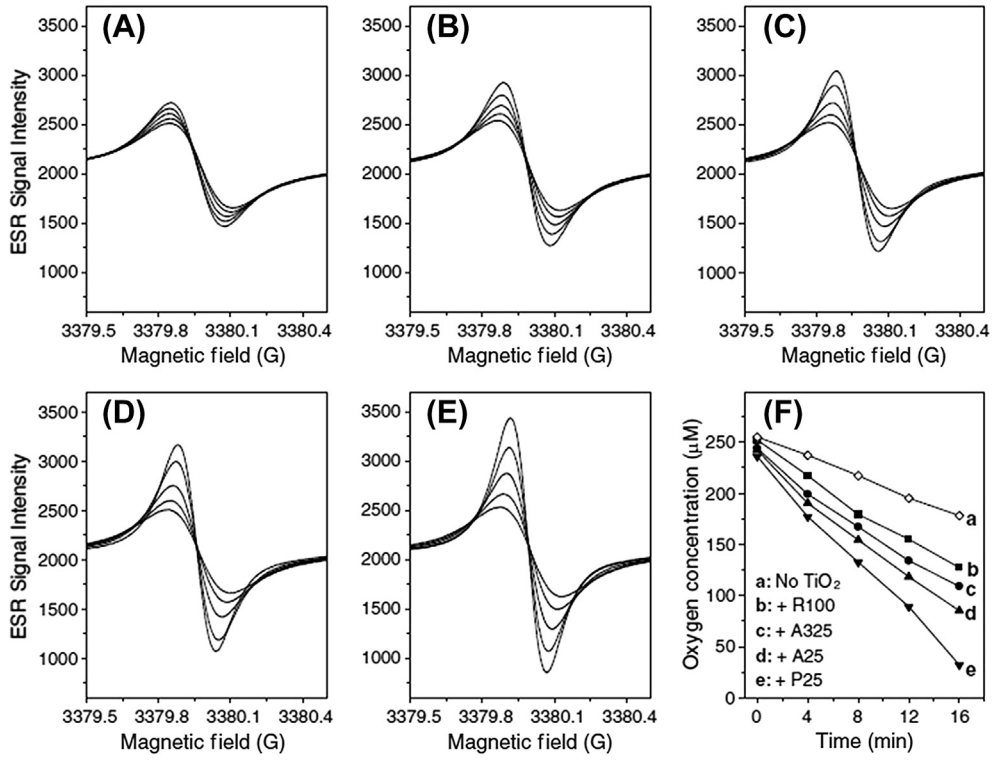

Fig. 10 – Effect of TiO_2 samples on lipid peroxidation in liposomes. Oxygen consumption was measured in a closed chamber using liposome suspensions and the spin label ^{15}N-PDT. The liposome sample contained 30 mg/mL Egg PC and 0.1mM ^{15}N-PDT spin label mixed with no TiO_2 (curve "a" in Fig. 10F), 0.03 mg/mL of R100 (curve "b" in Fig. 10F), 0.03 mg/mL of A325 (curve "c" in Fig. 10F), 0.03 mg/mL of A25 (curve "d" in Fig. 10F), and 0.03 mg/mL of P25 (curve "e" in Fig. 10F). Lipid peroxidation was initiated by UV (340 nm) irradiation [9]. ^{15}N-PDT = 4-oxo-2,2,6,6-tetramethyl piperidine-d_{16}-1-^{15}N-oxyl.

information on the rate of lipid oxidation; this can be obtained by assessing the variation in O_2 uptake with time, calculated from the line widths of the spin label.

We have used ESR oximetry in conjunction with the spin label CTPO to monitor the effect of Au NPs in triggering the production of oxygen under biologically relevant conditions [5]. Resolution of the superhyperfine structure of the low-field line of the ESR spectrum of CTPO strongly depends on the O_2 concentration in the sample solution. An increase in the oxygen concentration results in a progressive reduction of the superhyperfine structure, with the eventual loss of the hyperfine structure. As seen in Fig. 9, the structure of the ESR signal of spin label CTPO was affected by various conditions. An ESR signal with a typical sharp superhyperfine structure and a high intensity of hyperfine structure was observed in the control sample without catalysts, indicating a low concentration of oxygen. However, when Au NPs were added, the superhyperfine structures diminished along with a corresponding decreased signal intensity that suggests the formation of O_2. The superhyperfine splitting of spin label clearly diminished with increasing pH, especially in samples with pH ranging from 6.0 to 11.

It is well known that ROS can induce time-dependent peroxidation of the polyunsaturated lipids in plasma membrane. Yin et al [9] studied lipid peroxidation by UVA irradiation of nano-TiO_2 using ESR oximetry. Consumption of oxygen associated with lipid peroxidation was measured from the time-dependent narrowing of the ESR signal for the spin probe ^{15}N-PDT (Fig. 10). The narrowing of the ESR signal was accompanied by an increase in its peak height within the scan range. The final ESR signal intensities of R100, A325, A25, and P25 nano-TiO_2 samples were approximately 7.5%, 11.7%, 16.2%, and 26.3%, respectively, higher than the control (Fig. 10). The progressive increases in peak-to-peak signal intensity along with narrowing of the line width in each panel were due to time-dependent oxygen consumption associated with lipid peroxidation. Fig. 10F presents the data as a decrease in oxygen concentration, reflecting the variations in the slope (oxygen concentration vs. time) with different nano-TiO_2 species, which is in the following order: P25 > A25 > A325 > R100.

5. Conclusions

The production of ROS induced by nanomaterials is a double-edged sword, bringing not only the benefits of efficient nanomaterials for therapeutic treatment of diseases, but also possible health and environmental risks associated with them. Therefore, it is important to identify ROS for developing

nanomaterials for specific applications and understanding risks associated with their use. The use of ESR techniques to study ROS generation mediated by nanomaterials has several advantages compared to other techniques. Most importantly, ESR provides a more direct and chemically specific method for detecting ROS formation and identifying free radical species.

Because nanomaterials can affect cellular function through the production of ROS, ESR is an important technique used to study the free radical mechanisms of nanomaterial toxicity. In fact, the ability of nanomaterials to facilitate electron transfer, and thereby promote ROS generation, may be a fundamental property of these materials. It is still not clear whether and how the ROS production is associated with the physicochemical characteristics in terms of mechanisms and activity. For example, what factors cause the different type of ROS generated by different kinds of nanomaterials? Is there any dependence on the size, shape, or crystal facet of nanomaterials in the generation of ROS? In addition, how does ROS contribute to the toxicity of nanomaterials? To answer these questions, one requires to have not only a clear understanding of the mechanism of ROS generation in different types of nanomaterials, but also the knowledge of standard nanomaterials with well-controlled size, shape, composition, and surface states to compare their abilities in generating ROS.

Conflicts of interest

All authors declare no conflicts of interest.

Acknowledgments

This work was supported by a regulatory science grant under the US Food and Drug Administration (FDA) Nanotechnology CORES Program and by the Office of Cosmetics and Colors (CFSAN/FDA), and was supported in part by an appointment (W.H.) to the Research Program at the CFSAN administered by the ORISE. W.H. also acknowledges the support from the National Natural Science Foundation of China (grant no. 21303153). The authors deeply appreciate Dr Michael F. Santillo's critical review of the paper.

REFERENCES

[1] National Nanotechnology Initiative. http://www.nano.gov/nanotech-101. 2013.
[2] Minai L, Yeheskely-Hayon D, Yelin D. High levels of reactive oxygen species in gold nanoparticle-targeted cancer cells following femtosecond pulse irradiation. Sci Rep 2013;3:2146.
[3] Marambio-Jones C, Hoek EMV. A review of the antibacterial effects of silver nanomaterials and potential implications for human health and the environment. J Nanopart Res 2010;12:1531–51.
[4] He WW, Zhou YT, Wamer WG, et al. Mechanisms of the pH dependent generation of hydroxyl radicals and oxygen induced by Ag nanoparticles. Biomaterials 2012;33:7547–55.
[5] He WW, Zhou YT, Wamer WG, et al. Intrinsic catalytic activity of Au nanoparticles with respect to hydrogen peroxide decomposition and superoxide scavenging. Biomaterials 2013;34:765–73.
[6] Zhang W, Li Y, Niu JF, et al. Photogeneration of reactive oxygen species on uncoated silver, gold, nickel, and silicon nanoparticles and their antibacterial effects. Langmuir 2013;29:4647–51.
[7] Wang B, Yin JJ, Zhou XY, et al. Physicochemical origin for free radical generation of iron oxide nanoparticles in biomicroenvironment: catalytic activities mediated by surface chemical states. J Phys Chem C 2013;117:383–92.
[8] Vankayala R, Kuo CL, Sagadevan A, et al. Morphology dependent photosensitization and formation of singlet oxygen (1Δg) by gold and silver nanoparticles and its application in cancer treatment. J Mater Chem B 2013;1:4379–87.
[9] Yin JJ, Liu J, Ehrenshaft M, et al. Phototoxicity of nano titanium dioxides in HaCaT keratinocytes—Generation of reactive oxygen species and cell damage. Toxicol Appl Pharmacol 2012;263:81–8.
[10] Pan Y, Leifert A, Ruau D, et al. Gold nanoparticles of diameter 1.4 nm trigger necrosis by oxidative stress and mitochondrial damage. Small 2009;5:2067–76.
[11] Rahman MF, Wang J, Patterson TA, et al. Expression of genes related to oxidative stress in the mouse brain after exposure to silver-25 nanoparticles. Toxicol Lett 2009;87:15–21.
[12] Kalyanaraman B, Darley-Usmar V, Davies KJA, et al. Measuring reactive oxygen and nitrogen species with fluorescent probes: challenges and limitations. Free Radic Biol Med 2012;52:1–6.
[13] Chen X, Tian X, Shin I, et al. Fluorescent and luminescent probes for detection of reactive oxygen and nitrogen species. Chem Soc Rev 2011;40:4783–804.
[14] Kobayashi H, Guzman EG, Mahran AM, et al. Quality control of reactive oxygen species measurement by luminol-dependent chemiluminescence assay. J Androl 2001;22:568–74.
[15] Cheng ZH, Zhou HP, Yin JJ, et al. ESR estimation of hydroxyl radical scavenging capacity for lipophilic antioxidants. J Agric Food Chem 2007;55:3325–33.
[16] Cheng Z, Zhou H, Luther M, et al. Effects of wheat antioxidants on oxygen diffusion–concentration products in liposomes and key genes for cholesterol biosynthesis and metabolism in primary rat hepatocytes. J Agric Food Chem 2008;56:5033–42.
[17] Chiang LY, Lu FJ, Lin JT. Free-radical scavenging activity of water-soluble fullerenols. J Chem Soc Chem Commun 1995:1283–4.
[18] Chiang HM, Yin JJ, Xia Q, et al. Photoirradiation of azulene and guaiazulene—formation of reactive oxygen species and induction of lipid peroxidation. J Photochem Photobiol A 2010;211:123–8.
[19] Fu PP, Xia Q, Yin JJ, et al. Photodecomposition of retinyl palmitate and photobiological implications for the skin. Photochem Photobiol 2007;83:409–24.
[20] Fu PP, Chiang HM, Xia Q, et al. Quality assurance and safety of herbal dietary supplements. J Environ Sci Health C 2009;27:91–119.
[21] Li J, Liu H, Ramachandran S, et al. Grape seed proanthocyanidins ameliorate doxorubicin induced cardiotoxicity. Am J Chin Med 2010;38:569–84.
[22] Liang XJ, Meng H, Wang Y, et al. Metallofullerene nanoparticles circumvent tumor resistance to cisplatin by

reactivating endocytosis. Proc Natl Acad Sci 2010;107:7449–54.
[23] Moore J, Yin JJ, Yu L. Novel fluorometric assay for hydroxyl radical scavenging capacity (HOSC) estimation. J Agric Food Chem 2006;54:617–26.
[24] Su L, Yin JJ, Charles D, et al. Total phenolic contents, chelating capacities, and radical scavenging properties of black peppercorn, nutmeg, rosehip, cinnamon and oregano leaf. Food Chem 2007;100:990–7.
[25] Tolleson WH, Cherng SH, Xia Q, et al. Photodecomposition and phytotoxicity of natural retinoids. Int J Environ Res Public Health 2005;2:147–55.
[26] Wang CY, Wang SY, Yin JJ, et al. Enhancing antioxidant, antiproliferation, and free radical scavenging activities in strawberries with essential oils. J Agric Food Chem 2007;55:6527–32.
[27] Wang L, Wang S, Yin JJ, et al. Light-induced mutagenicity and genotoxicity/cytotoxicity of tamoxifen: a chemotherapeutic and chemopreventive agent. J Photochem Photobiol A Chem 2009;201:50–6.
[28] Wang C, Chen CT, Yin JJ. Effect of allyl isothiocyanate on antioxidants and fruit decay of blueberries. Food Chem 2010;120:199–204.
[29] Xia Q, Chou MW, Yin JJ, et al. Photoirradiation of representative polycyclic aromatic hydrocarbons and twelve isomeric methylbenz[a]anthracene with UVA light-formation of lipid peroxidation. Toxicol Ind Health 2006;22:147–56.
[30] Xia Q, Yin JJ, Cherng SH, et al. UVA photoirradiation of retinyl palmitate—formation of singlet oxygen and superoxide, and their role in induction of lipid peroxidation. Toxicol Lett 2006;163:30–43.
[31] Xia Q, Yin JJ, Wamer WG, et al. Photoirradiation of retinal palmitate in ethanol with ultraviolet light, formation of photodecomposition products, reactive oxygen species, and lipid peroxides. Int J Environ Res Public Health 2006;3:185–90.
[32] Xia Q, Yin JJ, Beland FA, et al. Photoirradiation of Aloe vera by UVA—formation of free radicals, singlet oxygen, superoxide, and induction of lipid peroxidation. Toxicol Lett 2007;168:165–75.
[33] Yin JJ, Kramer JKG, Yurawecz MP, et al. Effects of conjugated linoleic acid (CLA) isomers on oxygen diffusion–concentration products in liposomes and phospholipids solutions. J Agric Food Chem 2006;54:7287–93.
[34] Yin JJ, Yu LP, Yurawecz MP, et al. Antioxidative activity of CLA determined by ESR. In: Yurawecz MP, Kramer JKG, Pariza MW, Banni S, editors. Advance in conjugated linoleic acid researchvol. 3. Champaign, IL, USA: AOCS Press; 2006. p. 183–200.
[35] Yin JJ, Xia Q, Fu PP. UVA photoirradiation of anhydroretinol—formation of singlet oxygen and superoxide. Toxicol Ind Health 2007;23:625–31.
[36] Yin JJ, Fang L, Fu PP, et al. Inhibition of tumor growth by endohedral metallofullerenol nanoparticles optimized as reactive oxygen species scavenger. Mol Pharma 2008;74:1132–40.
[37] Yin JJ, Xia Q, Cherng SH, et al. UVA photoirradiation of oxygenated benz[a]anthracene and 3-methylcholanthene—generation of singlet oxygen and induction of lipid peroxidation. Int J Environ Res Public Health 2008;5:26–31.
[38] Yin JJ, Lao F, Fu PP, et al. The scavenging of reactive oxygen species and the potential for cell protection by functionalized fullerene materials. Biomaterials 2009;30:611–21.
[39] Zhao B, He YY, Bilski PJ, et al. Pristine (C_{60}) and hydroxylated [$C_{60}(OH)_{24}$] fullerene phototoxicity towards HaCaT keratinocytes: Type I vs Type II mechanisms. Chem Res Toxicol 2008;21:1056–63.
[40] Zhao BZ, He YY, Chignell CF, et al. Difference in phototoxicity of cyclodextrin complexed fullerene [(γ-CyD)$_2$/C60] and its aggregated derivatives towards human lens epithelial cells. Chem Res Toxicol 2009;22:660–7.
[41] Zhao B, Yin JJ, Bilski PJ, et al. Enhanced photodynamic efficacy towards melanoma cells by encapsulation of Pc4 in silica nanoparticles. Toxicol Appl Pharma 2009;241:163–72.
[42] Yin JJ, Fu PP, Lutterodt H, et al. Dual role of selected antioxidants found in dietary supplements: crossover between anti- and pro-oxidant activities in the presence of copper. J Agric Food Chem 2012;60:2554–61.
[43] Zhou K, Yin JJ, Yu L. ESR determination of the reactions between wheat phenolic acids and free radicals or transition metals. Food Chem 2006;95:446–57.
[44] Yin JJ, Fu PP. Application of electron spin resonance to study food antioxidative and prooxidative activates. In: Gudjonsdottir M, Belton P, Webb G, editors. Magnetic resonance in food science: challenges in a changing world. Cambridge: RSC; 2009. p. 213–21.
[45] Yin JJ, Xia Q, Lutterodt H, et al. Application of electron spin resonance spectroscopy to study dietary ingredients and supplements – dual antioxidant and prooxidant functions of retinyl palmitate. In: Renou JP, Webb GA, Belton PS, editors. Magnetic resonance in food science: an exciting future. RSC 2011. p. 126–35.
[46] Yin JJ, Zhao B, Xia Q, et al. Electron spin resonance spectroscopy for studying the generation and scavenging of reactive oxygen species by nanomaterials. In: Liang X-J, editor. Nanopharmaceuticals: the potential application of nanomaterials. Chapter 14. Singapore: World Scientific Publishing Company; 2012. p. 375–400.
[47] Schweiger A, Jeschke G. Principles of pulse electron paramagnetic resonance. New York: Oxford University Press; 2001.
[48] Janzen EG. Electron spin resonance. Anal Chem 1974;46:478–90.
[49] Morton JR. Electron spin resonance spectra of oriented radicals. Chem Rev 1964;64:453–71.
[50] Buettner GR. Spin trapping: ESR parameters of spin adducts. Free Radic Biol Med 1987;3:259–303.
[51] Kawasaki K, Yin JJ, Subczynski WK, et al. Pulse EPR detection of lipid exchange between protein-rich raft and bulk domains in the membrane: methodology development and its application to studies of influenza viral membrane. Biophys J 2001;80:738–48.
[52] Marsh D, Kurad D, Livshits VA. High-field spin-label EPR of lipid membranes. Magn Reson Chem 2005;43:S20–5.
[53] Zhao H, Joseph J, Zhang H, et al. Synthesis and biochemical applications of a solid cyclic nitrone spin trap: a relatively superior trap for detecting superoxide anions and glutathiyl radicals. Free Radic Biol Med 2001;31:599–606.
[54] Dikalov S, Skatchkov M, Bassenge E. Spin trapping of superoxide radicals and peroxynitrite by 1-hydroxy-3-carboxy-pyrrolidine and 1-hydroxy-2,2,6,6-tetramethyl-4-oxo-piperidine and the stability of corresponding nitroxyl radicals towards biological reductants. Biochem Biophys Res Commun 1997;231:701–4.
[55] Hubbell WL, McConnell HM. Spin-label studies of the excitable membranes of nerve and muscle. Proc Natl Acad Sci 1968;61:12–6.

[56] Zhou YT, Yin JJ, Lo YM. Application of ESR spin label oximetry in food science. Magn Reson Chem 2011;49:S105–12.
[57] Froncisz W, Lai CS, Hyde JS. Spin-label oximetry: kinetic study of cell respiration using a rapid-passage T_1-sensitive electron spin resonance display. Proc Natl Acad Sci 1985;82:411–5.
[58] Fu PP, Xia QS, Hwang HM, et al. Mechanisms of nanotoxicity: generation of reactive oxygen species. J Food Drug Anal 2014;22:64–75.
[59] Wardman P, Candeias LP. Fenton chemistry: an introduction. Radiat Res 1996;145:523–53.
[60] Choi O, Hu Z. Size dependent and reactive oxygen species related nanosilver toxicity to nitrifying bacteria. Environ Sci Technol 2008;42:4583–8.
[61] Carlson C, Hussain SM, Schrand AM, et al. Unique cellular interaction of silver nanoparticles: size-dependent generation of reactive oxygen species. J Phys Chem B 2008;112:13608–19.
[62] Piao MJ, Kang KA, Lee IK, et al. Silver nanoparticles induce oxidative cell damage in human liver cells through inhibition of reduced glutathione and induction of mitochondria-involved apoptosis. Toxicol Lett 2011;201:92–100.
[63] Kim JS, Kuk E, Yu KN, et al. Antimicrobial effects of silver nanoparticles. Nanomedicine 2007;3:95–101.
[64] AshaRani PV, Mun GLK, Hande MP, et al. Cytotoxicity and genotoxicity of silver nanoparticles in human cells. ACS Nano 2009;3:279–90.
[65] Hwang ET, Lee JH, Chae YJ, et al. Analysis of the toxic mode of action of silver nanoparticles using stress-specific bioluminescent bacteria. Small 2008;4:746–50.
[66] Ono Y, Matsumura T, Kitajima N, et al. Formation of superoxide during the decomposition of hydrogen peroxide on supported metals. J Phys Chem 1977;81:1307–11.
[67] Li L, Sun J, Li X, et al. Controllable synthesis of monodispersed silver nanoparticles as standards for quantitative assessment of their cytotoxicity. Biomaterials 2012;33:1714–21.
[68] Foldbjerga R, Olesena P, Hougaardb M, et al. PVP-coated silver nanoparticles and silver ions induce reactive oxygen species, apoptosis and necrosis in THP-1 monocytes. Toxicol Lett 2009;190:156–62.
[69] Oo MKK, Yang YM, Hu Y, et al. Gold nanoparticle-enhanced and size-dependent generation of reactive oxygen species from protoporphyrin IX. ACS Nano 2012;6:1939–47.
[70] Misawa M, Takahashi J. Generation of reactive oxygen species induced by gold nanoparticles under X-ray and UV irradiations. Nanomedicine 2011;7:604–14.
[71] Mepedović S, Locke BR. Platinum catalysed decomposition of hydrogen peroxide in aqueous-phase pulsed corona electrical discharge. Appl Catal B Environ 2006;67:149–59.
[72] Krylova G, Dimitrijevic NM, Talapin DV, et al. Probing the surface of transition-metal nanocrystals by chemiluminescence. J Am Chem Soc 2010;132:9102–10.
[73] Xu CJ, Yuan ZL, Kohler N, et al. FePt nanoparticles as an Fe reservoir for controlled Fe release and tumor inhibition. J Am Chem Soc 2009;131:15346–51.
[74] Shi M, Kwon HS, Peng Z, et al. Effects of surface chemistry on the generation of reactive oxygen species by copper nanoparticles. ACS Nano 2012;6:2157–64.
[75] Rushton EK, Jiang J, Leonard SS, et al. Concept of assessing nanoparticle hazards considering nanoparticle dosemetric and chemical/biological response metrics. J Toxicol Environ Health A 2010;73:445–61.
[76] Jose GP, Santra S, Mandal SK, et al. Singlet oxygen mediated DNA degradation by copper nanoparticles: potential towards cytotoxic effect on cancer cells. J Nanobiotechnol 2011;9:9.
[77] Keenan CR, Sedlak DL. Factors affecting the yield of oxidants from the reaction of nanoparticulate zero-valent iron and oxygen. Environ Sci Technol 2008;42:1262–7.
[78] Keenan CR, Sedlak DL. Ligand-enhanced reactive oxidant generation by nanoparticulate zero-valent iron and oxygen. Environ Sci Technol 2008;42:6936–41.
[79] Keenan CR, Goth-Goldstein R, Lucas D, et al. Oxidative stress induced by zero-valent iron nanoparticles and Fe(II) in human bronchial epithelial cells. Environ Sci Technol 2009;43:4555–60.
[80] Kim JY, Park HJ, Lee C, et al. Inactivation of *Escherichia coli* by nanoparticulate zerovalent iron and ferrous ion. Appl Environ Microbiol 2010;76:7668–70.
[81] Chen Y, Cao H, Shi W, et al. Fe–Co bimetallic alloy nanoparticles as a highly active peroxidase mimetic and its application in biosensing. Chem Commun 2013;49:5013–5.
[82] Peters K, Unger RE, Gatti AM, et al. Metallic nanoparticles exhibit paradoxical effects on oxidative stress and pro-inflammatory response in endothelial cells *in vitro*. Int J Immunopathol Pharmacol 2007;20:685–95.
[83] Ahmad J, Alhadlaq HA, Siddiqui MA, et al. Concentration-dependent induction of reactive oxygen species, cell cycle arrest and apoptosis in human liver cells after nickel nanoparticles exposure. Environ Toxicol 2013. http://dx.doi.org/10.1002/tox.21879.
[84] Ahamed M. Toxic response of nickel nanoparticles in human lung epithelial A549 cells. Toxicol In Vitro 2011;25:930–6.
[85] Eustis S, El-Sayed MA. Why gold nanoparticles are more precious than pretty gold: noble metal surface plasmon resonance and its enhancement of the radiative and nonradiative properties of nanocrystals of different shapes. Chem Soc Rev 2006;35:209–17.
[86] Willets KA, Duyne RPV. Localized surface plasmon resonance spectroscopy and sensing. Annu Rev Phys Chem 2007;58:267–97.
[87] Lipinski B. Hydroxyl radical and its scavengers in health and disease, oxidative medicine and cellular longevity. Oxid Med Cell Longev 2011;2011:809696.
[88] Sies H. Strategies of antioxidant defense. Eur J Biochem 1993;215:213–9.
[89] Wamer WG, Yin JJ, Wei RR. Oxidative damage to nucleic acids photosensitized by titanium dioxide. Free Radic Biol Med 1997;23:851–8.
[90] Wamer WG, Yin JJ. Photocytotoxicity in human dermal fibroblasts elicited by permanent makeup inks containing titanium dioxide. J Cosmet Sci 2011;62:535–47.
[91] Wang CC, Wang S, Xia Q, et al. Phototoxicity of zinc oxide nanoparticles in HaCaT keratinocytes—generation of oxidative DNA damage during UVA and visible light irradiation. J Nanosci Nanotechnol 2013;13:3880–8.
[92] Chen ZW, Yin JJ, Zhou YT, et al. Dual enzyme-like activities of iron oxide nanoparticles and their implication for diminishing cytotoxicity. ACS Nano 2012;6:4001–12.
[93] Ge CC, Li Y, Yin JJ, et al. The contributions of metal impurities and tube structure to the toxicity of carbon nanotube materials. NPG Asia Materials 2012;4:e32.
[94] Zhang WD, Wang C, Li ZJ, et al. Unraveling stress-induced toxicity properties of graphene oxide and the underlying mechanism. Adv Mater 2012;24:5391–7.

[95] Harbour JR, Hair ML. Superoxide generation in the photolysis of aqueous cadmium sulfide dispersions. Detection by spin trapping. J Phys Chem 1977;81:1791–3.
[96] Wang WJ, Ng TW, Ho WK, et al. $CdIn_2S_4$ microsphere as an efficient visible-light-driven photocatalyst for bacterial inactivation: Synthesis, characterizations and photocatalytic inactivation mechanisms. Appl Catal B 2013;129:482–90.
[97] Zhao K, Zhang LZ, Wang J, et al. Surface structure-dependent molecular oxygen activation of BiOCl single-crystalline nanosheets. J Am Chem Soc 2013;135:15750–3.
[98] Yamamoto Y, Imai N, Mashima R, et al. Singlet oxygen from irradiated titanium dioxide and zinc oxide. Methods Enzymol 2000;319:29–37.